

# **A High Performance All-Solid-State Battery with Ni-Rich NCM Cathode Coated by ALD and Lithium Thiophosphate Solid Electrolyte**

David Kitsche,<sup>†</sup> Yushu Tang,<sup>‡</sup> Yuan Ma,<sup>†</sup> Damian Goonetilleke,<sup>†</sup> Joachim Sann,<sup>#</sup> Felix Walther,<sup>#</sup> Matteo Bianchini,<sup>†,§</sup> Jürgen Janek,<sup>†,#,\*</sup> and Torsten Brezesinski<sup>†,\*</sup>

<sup>†</sup> Battery and Electrochemistry Laboratory, Institute of Nanotechnology, Karlsruhe Institute for Technology (KIT), Hermann-von-Helmholtz-Platz 1, 76344 Eggenstein-Leopoldshafen, Germany.

<sup>‡</sup> Institute of Nanotechnology, Karlsruhe Institute for Technology (KIT), Hermann-von-Helmholtz-Platz 1, 76344 Eggenstein-Leopoldshafen, Germany.

<sup>#</sup> Institute of Physical Chemistry & Center for Materials Science (ZfM/LaMa), Justus-Liebig-University Giessen, Heinrich-Buff-Ring 17, 35392 Giessen, Germany.

<sup>§</sup> BASF SE, Carl-Bosch-Str. 38, 67056 Ludwigshafen, Germany.

## **Abstract**

Achieving compatibility between cell components is one of the major challenges for the widespread adoption of bulk-type solid-state batteries. In particular, superionic lithium thiophosphate solid electrolytes suffer from oxidation at high voltages when interfaced with state-of-the-art cathode materials. Here, we report on atomic layer deposition (ALD) of conformal  $\text{HfO}_2$  nanocoatings onto  $\text{LiNi}_{0.85}\text{Co}_{0.10}\text{Mn}_{0.05}\text{O}_2$  (NCM-851005) cathode material. Based on electrochemical testing in high-loading (pellet-stack) solid-state battery cells, we demonstrate the positive effect of ALD  $\text{HfO}_2$  coating on the cyclability and stability of NCM-851005. Modification of the coating morphology by post annealing further improved the cycling performance considerably, especially the Coulombic efficiency in the initial cycles and the rate capability. The results demonstrate the ability of ALD to produce high-quality surface films on industrially relevant electrode materials, thus providing a suitable platform for systematic investigations into the functionality of protective coatings in solid-state and other batteries.

## **Keywords**

solid-state battery, atomic layer deposition, layered Ni-rich oxide cathode, argyrodite solid electrolyte, protective coating, interfaces

## 1. Introduction

Solid-state batteries (SSBs) are among the prime candidates to replace conventional lithium-ion batteries (LIBs) for application in electric vehicles. This is due, in part, to the fact that LIBs are approaching their limits in terms of gravimetric and volumetric energy density in the near term.<sup>1–3</sup> Among the conceivable solid electrolytes (SEs), lithium thiophosphates stand out, as they exhibit the highest room-temperature ionic conductivities achieved so far while at the same time offering favorable mechanical properties.<sup>1,4–6</sup> However, their main drawback is a narrow stability window, giving rise to reduction (e.g., when paired with a lithium-metal anode) and oxidation reactions at low and high voltages, respectively. This is the case particularly at the voltages to which high-capacity cathode active materials (CAMs), such as layered lithium metal oxides of the form  $\text{LiNi}_x\text{Co}_y\text{Mn}_z\text{O}_2$  (referred to as NCM or NMC), are being cycled. The side reactions occurring at the interface between the SE and CAM particles (and/or the conductive additive) during battery operation lead to the formation of detrimental degradation products and therefore to impedance growth and capacity fading.<sup>5,7–9</sup> This emphasizes the need for protective CAM coatings which, above all, should serve as an ion-conducting but electron-blocking layer. However, the surface shell must not be completely electronically insulating, as otherwise sufficient electronic percolation in the electrode cannot be achieved.<sup>8</sup>

In recent years, several studies have demonstrated the beneficial effects of CAM coatings in SSBs (evident from improvements in cycling stability and rate capability, for example),<sup>8</sup> with the vast majority focusing on Li-containing ternary oxides, such as  $\text{LiNbO}_3$  or  $\text{Li}_4\text{Ti}_5\text{O}_{12}$ , applied by wet-chemical deposition techniques.<sup>10–12</sup> Although the latter methods are versatile, cost-efficient, and easy to implement, they provide only limited control over coating thickness and morphology.<sup>13</sup> Hence, the quest for highly effective coating materials and advanced coating technologies is ongoing.

Atomic layer deposition (ALD) allows preparing atomically thin, conformal coatings on substrates with complex surfaces. The technique has been extensively applied in the field of LIBs.<sup>13–17</sup> Several promising CAM coatings based on  $\text{LiMO}_x$  (e.g., with  $M = \text{Nb}$ ,<sup>19</sup>  $\text{Ta}$ ,<sup>20</sup>  $\text{P}^{21}$ ) have been successfully produced by means of ALD. However, few examples exist in the literature on the use of ALD-modified CAMs in bulk-type SSBs.<sup>8,22</sup> Herein, we report on the coating of a Ni-rich NCM CAM,  $\text{LiNi}_{0.85}\text{Co}_{0.1}\text{Mn}_{0.05}\text{O}_2$  (NCM-851005), with  $\text{HfO}_2$ .  $\text{HfO}_2$  exhibits chemical and structural similarities to  $\text{ZrO}_2$ , from which a number of protective CAM coatings for SSB applications have been derived.<sup>23–26</sup> ALD of  $\text{HfO}_2$  is a well-established process. Note that  $\text{HfO}_2$  thin films are widely used as high- $k$  dielectrics in the semiconductor industry. One of the most common precursors is tetrakis(ethylmethylamido)hafnium(IV) (TEMAH), which can be employed in combination with  $\text{H}_2\text{O}$  or  $\text{O}_3$  as the oxidant.<sup>27–31</sup>

In this work, we describe the preparation of  $\text{HfO}_2$ -coated NCM-851005 CAM via ALD of TEMAH/ $\text{O}_3$  and characterize the surface layer using different techniques. The positive effect of the coating, especially after annealing, on the electrochemical performance of NCM-851005 in thiophosphate-based SSB cells is also demonstrated.

## 2. Experimental Section

**2.1. Atomic Layer Deposition (ALD).** Prior to ALD coating,  $\text{LiNi}_{0.85}\text{Co}_{0.10}\text{Mn}_{0.05}\text{O}_2$  (NCM-851005; BASF SE) CAM was heated in  $\text{O}_2$  flow at  $750\text{ }^\circ\text{C}$  for 3 h to reduce the amount of residual surface carbonates. The heating and cooling rates were set to  $5\text{ }^\circ\text{C}/\text{min}$ . For the coating process, 2 g of NCM-851005 was encased in a gas-permeable powder holder and introduced into the ALD reactor (Picosun). After 1 h stabilization at  $250\text{ }^\circ\text{C}$ , the reactor was flushed with  $\text{N}_2$ . A typical ALD process comprised 20 cycles, consisting of a pulse sequence for  $\text{O}_3$  (ozone generator from IN USA Inc.) followed by the same sequence for  $\text{Hf}[\text{N}(\text{CH}_2\text{CH}_3)(\text{CH}_3)]_4$  (TEMAH; 99.99%, Sigma-Aldrich, precursor container heated at  $105\text{ }^\circ\text{C}$ ). It contained 100 pulses of 0.1 s duration, each followed by 2 s reactor purging and 60 s purging after the last pulse. This sequence was carried out once for  $\text{O}_3$  before commencing the 20 ALD cycles. The  $\text{N}_2$  carrier-gas flow in the TEMAH and ozone lines was set to 200 sccm. Finally, the  $\text{HfO}_2$ -coated NCM-851005 CAM was heated in  $\text{O}_2$  flow at  $400\text{ }^\circ\text{C}$  for 30 min, with heating and cooling rates set to  $10\text{ }^\circ\text{C}/\text{min}$ .

**2.2. Elemental Analysis.** For elemental analysis, ALD-coated NCM-851005 CAM was dissolved in acid using a graphite furnace. The Hf content was determined by inductively coupled plasma-optical emission spectroscopy (ICP-OES) using a Thermo Fisher Scientific iCAP 7600 DUO. The carbon content was probed using a CS analyzer. Mass fractions represent the mean of three independent measurements.

**2.3. X-Ray Diffraction (XRD).** XRD data were collected using a STOE Stadi P diffractometer with a DECTRIS MYTHEN 1K strip detector in Debye-Scherrer geometry. The instrument uses a Mo anode, which provides a wavelength of  $\lambda = 0.70926\text{ \AA}$ . The instrumental contribution to the peak broadening was obtained by measuring a NIST 640f Si standard reference material (SRM) as a line broadening reference. Rietveld refinement was performed using GSAS-II.<sup>32</sup> For refinement of NCM structural models against the diffraction data, the scale factor, zero shift, and crystallite size broadening parameters were allowed to vary. A fixed background was fitted to the data using a Chebyshev polynomial function with 16 terms. In the structural model, the unit cell parameters, the oxygen z-coordinate, and the atomic displace parameters (isotropic,  $u_{\text{iso}}$ ) for each site were refined. Atoms occupying the same site were constrained to have the same atomic parameters, and site occupancy factors (SOFs) were constrained such that each site remained fully occupied.

**2.4. X-Ray Photoelectron Spectroscopy (XPS).** XPS measurements were carried out with a PHI VersaProbe II instrument (ULVAC-PHI, Inc.) using monochromatic Al  $\text{K}\alpha$  radiation ( $\lambda = 1486.6\text{ eV}$ ). The power of the X-ray source was set to 100 W. The powder samples were pressed into pellets and mounted on the sample holder with insulating double sided tape (inert sample transfer). The examined area had a size of  $1.3\text{ mm} \times 0.1\text{ mm}$ . For survey and detail spectra, pass energies of 93.9 and 23.5 eV, respectively, were used. For charge neutralization, the PHI dual-beam charge neutralization was employed, consisting of a 20 nA, 10 V Ar-ion beam in combination with a 20  $\mu\text{A}$ , 3 V electron beam and effectively pinning the sample potential at  $-3\text{ V}$  versus ground potential. Data evaluation was carried out with the software CasaXPS

(version 2.3.18, Casa Software Ltd.). The spectra were calibrated in relation to the signal of adventitious carbon at 284.8 eV. A Shirley background was used, and the spectra were fitted with a GL line shape.

**2.5. Scanning Electron Microscopy (SEM).** SEM and energy-dispersive X-ray spectroscopy (EDS) were carried out at an accelerating voltage of 20 kV using a LEO-1530 electron microscope (Carl Zeiss AG) with a field emission source. Cross-sectional SEM images were taken from manually fractured pellets, harvested from SSB cells before/after cycling.

**2.6. Transmission Electron Microscopy (TEM).** NCM-851005 CAM samples were investigated using Tecnai F20 ST and Themis-Z microscopes (Thermo Fisher Scientific) at accelerating voltages of 200 and 300 kV, respectively. Elemental maps of particle cross sections were acquired by EDS on the Themis-Z microscope at 300 kV with a Super-X EDS detector. Sample cross sections were prepared using a focused Ga-ion beam (FIB) in an FEI Strata 400 at 30 kV. Carbon layers were deposited by electron/ion-beam-induced deposition to protect the coating during sample preparation and processing. The carbon tape where the NCM-851005 CAM particles were put on was also thinned to characterize the coating.

**2.7. Electrode Composites.** Cathode composite was prepared by mixing the NCM-851005 CAM, Li<sub>6</sub>PS<sub>5</sub>Cl (LPSCI; NEI Corp.) SE, and Super C65 carbon black additive (Timcal) 69:30:1 by weight using 10 zirconia balls in a planetary mill (Fritsch) at 140 rpm for 30 min under an Ar atmosphere. Using the same procedure, anode composite was prepared from carbon-coated Li<sub>4</sub>Ti<sub>5</sub>O<sub>12</sub> (LTO; NEI Corp.), LPSCI, and Super C65 carbon black at a weight ratio of 30:60:10.

**2.8. Solid-State Battery Cell Assembly and Testing.** The electrochemical performance of the uncoated and HfO<sub>2</sub>-coated NCM-851005 CAMs was tested in SSB cells using a customized setup comprising a polyether ether ketone (PEEK) sleeve and two stainless steel dies. 10 mm-diameter pellet stacks were produced by first cold pressing an amount of 100 mg Li<sub>6</sub>PS<sub>5</sub>Cl SE at a uniaxial pressure of 62 MPa to prepare the separator layer. Subsequently, 65 mg anode composite and 12 mg cathode composite ( $\sim 2.9$  mAh/cm<sup>2</sup> for  $q_{th} = 274$  mAh/g<sub>CAM</sub>) were added on either side, and the stack was pressed at 437 MPa. The final cells were galvanostatically cycled at 45 °C in a voltage range between  $\sim 2.9$  and 4.3 V versus Li<sup>+</sup>/Li while maintaining a uniaxial pressure of 81 MPa. Cycling stability tests were carried out at 0.5C (1C = 190 mA/g<sub>CAM</sub>) for 60 cycles. Rate performance tests were carried out at 0.1C, 0.2C, 0.5C, and 1C, with two charge/discharge cycles at each C-rate. Results are averaged from at least three independent measurements.

**2.9. Li-Ion Battery (LIB) Cell Testing.** Cathodes for testing in LIB coin cells consisted of the NCM-851005 CAM, Super C65 carbon black, and polyvinylidene fluoride (PVDF) binder in a 94:3:3 weight ratio. A slurry based on N-methyl-2-pyrrolidone (NMP) was cast onto Al foil, vacuum-dried overnight at 120 °C, and then calendared at 15 N/mm. 12 mm-diameter circular electrodes with an areal loading of 10 mg<sub>CAM</sub>/cm<sup>2</sup> were punched out from the as-prepared tapes and used to assemble 2032 coin cells. The cells used a glass fiber separator (GF/D; Whatman), 100  $\mu$ l LP57 electrolyte (1 M LiPF<sub>6</sub>

in 3:7 by weight ethylene carbonate and ethyl methyl carbonate; BASF SE), and a Li-metal anode (Albemarle Germany GmbH). They were galvanostatically cycled at 45 °C in the same voltage window (2.9-4.3 V vs Li<sup>+</sup>/Li) at 0.1C, 0.2C, 0.5C, and 1C, with two charge/discharge cycles at each C-rate, followed by 0.2C (1C = 225 mA/g<sub>CAM</sub>).

**2.10. Electrochemical Impedance Spectroscopy (EIS).** EIS was carried out at frequencies ranging from 7 MHz to 100 mHz with an amplitude of 10 mV using a VMP3 impedance analyzer (Bio-Logic Science Instruments Ltd.).

### 3. Results and Discussion

#### 3.1. Surface Modification via ALD Coating

The as-received NCM-851005 CAM was first heated in O<sub>2</sub> flow at 750 °C for 3 h to minimize the impact of detrimental surface carbonates remaining from the synthesis.<sup>33</sup> According to elemental analysis, this treatment led to a decrease in carbon content from 0.23 to 0.09 wt %, which translates to a decrease in carbonate content from 1.38 to 0.54 wt % assuming that all carbon is present in the form of Li<sub>2</sub>CO<sub>3</sub>.

Initial experiments showed that HfO<sub>2</sub> can be deposited onto NCM-851005 using H<sub>2</sub>O or O<sub>3</sub> as a counter reactant. It should be noted that exposure of layered Ni-rich oxide CAMs to ambient atmosphere typically leads to some degree of degradation.<sup>34</sup> However, exposure to H<sub>2</sub>O in the ALD process at a reactor temperature of 250 °C did not severely affect the electrochemical performance of the NCM-851005 in SSB cells. Regardless, H<sub>2</sub>O is present in the ALD reactor, as it is formed as a side product when using O<sub>3</sub> as the counter reactant, but in much lower amounts.<sup>30</sup> Nevertheless, based on promising initial electrochemical testing results (**Figure S1**), O<sub>3</sub> was selected as oxidant in this study.

ICP-OES results indicated that the amount of deposited material, and therefore the coating thickness, can be tailored by the number of ALD cycles (**Figure S2**), as expected. The growth rate was found to increase with increasing ALD cycles. This suggests slower or less preferred deposition onto the NCM-851005 CAM than onto an already formed HfO<sub>2</sub> film. Similar behavior has been observed for other ALD processes in the past and is presumably due to the different number of reactive surface sites as the deposition progresses.<sup>35</sup> The sample containing 0.61 wt % HfO<sub>2</sub> (0.52 wt % Hf from ICP-OES), resulting from 20 TEMAH/O<sub>3</sub> cycles (100 pulses of 0.1 s duration), was among the best-performing CAMs in the investigated thickness or coating content range (**Figure S3**) and studied in more detail in the present work.

From the total surface area  $A$ , the mass fraction  $w$  and density  $\rho$  of the deposited material, and the total mass  $m$  of the sample, the coating thickness  $t$  can be estimated according to:  $t = \frac{w}{\rho \cdot A} \cdot m$ . Using the Brunauer-Emmett-Teller (BET) surface area of the NCM-851005 CAM ( $A_{\text{BET}} = 0.71 \text{ m}^2/\text{g}$ ) and the crystallographic density of monoclinic HfO<sub>2</sub> ( $\rho = 10.1 \text{ g}/\text{cm}^3$ ), this yields a coating thickness of 0.86 nm, which in turn corresponds to an average growth per cycle of 0.43 Å. However, because the actual density of the deposited HfO<sub>2</sub> and the total substrate area are probably somewhat

lower, the average coating thickness and growth rate are expected to be higher, and thus the estimates should be seen as lower bounds only.

XRD was used to examine potential effects of the ALD process on the crystal structure of NCM-851005 (**Figure S4**). All of the observed diffraction peaks before and after coating, as well as after annealing at 400 °C for 30 min in an oxygen atmosphere, could be accounted for using the expected hexagonal  $\alpha$ -NaFeO<sub>2</sub>-type structure with the space group  $R\bar{3}m$  (**Figure S4a**). Rietveld refinement confirmed that the change in structural parameters upon coating/annealing is negligible (**Figure S4b, Table S1**).

Furthermore, XPS was used to study the influence of the coating process on the NCM-851005 CAM. **Figure S5** shows XP spectra of the Ni 2p and O 1s core level regions. Both ALD (when using H<sub>2</sub>O or O<sub>3</sub> as the counter reactant) and the post-annealing step did not lead to a notable modification/degradation of the CAM surface. Apart from increased quantities of carbonate or related species, the data only suggest the presence of a slightly oxygen-depleted layer.

Next, electron microscopy was used to probe the morphology of the coated CAM and the microstructure of the coating. **Figure 1** presents SEM, high-angle annular dark-field scanning transmission electron microscopy (HAADF STEM), and high-resolution TEM (HRTEM) data for the as-prepared HfO<sub>2</sub>-coated NCM-851005. SEM investigations did not reveal major changes in CAM morphology during either the ALD or annealing processes (**Figure 1a, Figure S6**). Yet, bright spots were visible on the NCM-851005 particles, and a slightly roughened surface texture indicated the presence of a shell. TEM was also used to reveal the microstructure of the HfO<sub>2</sub> coating. **Figure 1b** shows a thin layer, conformally covering the outer surface of an NCM-851005 particle. As expected, it appeared bright in HAADF STEM imaging due to the high atomic number of Hf. Interestingly, the coating consisted of nanocrystals with a size of ~3 nm (**Figure 1c**). These nanoparticles were identified to have a monoclinic baddeleyite-type structure with the space group  $P2_1/c$ , which is the common low-temperature phase of HfO<sub>2</sub> (**Figure S7**).<sup>36</sup> Although such a morphology differs from the well-known 2-dimensional layer-by-layer (Frank-van der Merwe) growth, nanoparticle formation by ALD has been previously reported.<sup>37</sup> The latter can result from incomplete reaction of the ALD precursor(s) with the available surface sites and preferential chemisorption on already deposited material (island or Volmer-Weber growth). Preferred deposition onto transition-metal sites has been shown in a recent study on the non-uniform growth of ALD alumina thin films on NCM111 (33% Ni content).<sup>38</sup>

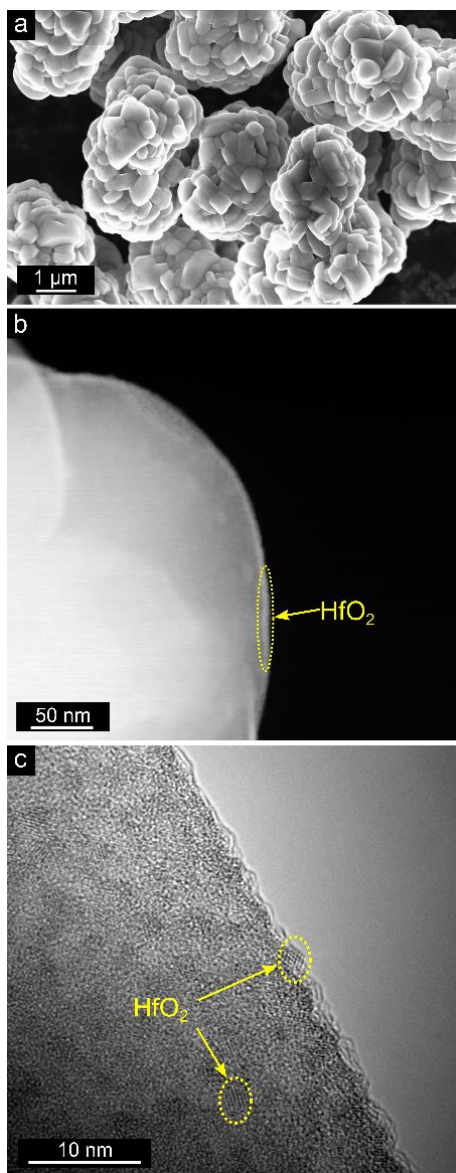


**Figure 1.** Electron microscopy of the as-prepared HfO<sub>2</sub>-coated NCM-851005 CAM. (a) SEM image demonstrating preserved CAM morphology after coating. (b) HAADF STEM image showing the coating as a thin surface shell. (c) HRTEM image revealing the presence of monoclinic HfO<sub>2</sub> nanocrystals on the surface.

**Figure 2** shows the HfO<sub>2</sub>-coated NCM-851005 CAM after annealing at 400 °C. Unlike for the as-prepared sample, no distinct coating nanoparticles were found on the surface, as can be seen from **Figure 2a**. Furthermore, the surface appeared smoother than before the heating. These results suggest that the HfO<sub>2</sub> layer densifies and spreads more evenly on the particle surface during the post-treatment process. The XP spectra of the Hf 4d and 4f core level regions were similar before and after annealing (**Figure S8**). Although there is no direct proof of significant Li incorporation into the HfO<sub>2</sub> layer, slight peak shifts (by ~0.15 and 0.25 eV for the Hf 4d and 4f data, respectively, relative to the as-prepared HfO<sub>2</sub>-coated NCM-851005) are indicative of increased Li/Hf interactions for the annealed CAM. In a recent study on Al<sub>2</sub>O<sub>3</sub>-coated NCM-701515, comparable (Al 2p) peak shifts to lower binding energies have been

ascribed to the formation of an amorphous  $\text{Al}_2\text{O}_3/\text{LiAlO}_2$  surface layer at 600 °C.<sup>39</sup> To gain more detailed information on the coating after annealing, FIB-cut cross sections were examined by TEM. **Figure 2b** shows a HAADF STEM image and corresponding elemental maps confirming that Hf accumulates at the particle surface. The coating thickness was measured to be in the range between 2 and 3 nm (**Figure S9**), corresponding to a growth rate of 1.0 to 1.5 Å per ALD cycle. Hence, the actual coating thickness is about three times larger than the above estimate. EDS also showed that virtually no Hf signal emerges from regions 5 to 10 nm away from the surface, thereby indicating that bulk diffusion can be ruled out (**Figure S10**). This was somewhat expected considering the ionic radius and charge of  $\text{Hf}^{4+}$ , as well as the relatively low annealing temperature. Elemental mapping further revealed that the primary particle surface in the interior of the secondary particles remains free of deposit (**Figure S11**). Coating of the interior could possibly be achieved to some extent, depending on the residual porosity, by altering the ALD conditions (e.g., using longer precursor pulse durations). However, regarding the application in SSBs, this is not important, as the inner primary particles are not in direct contact with the SE.

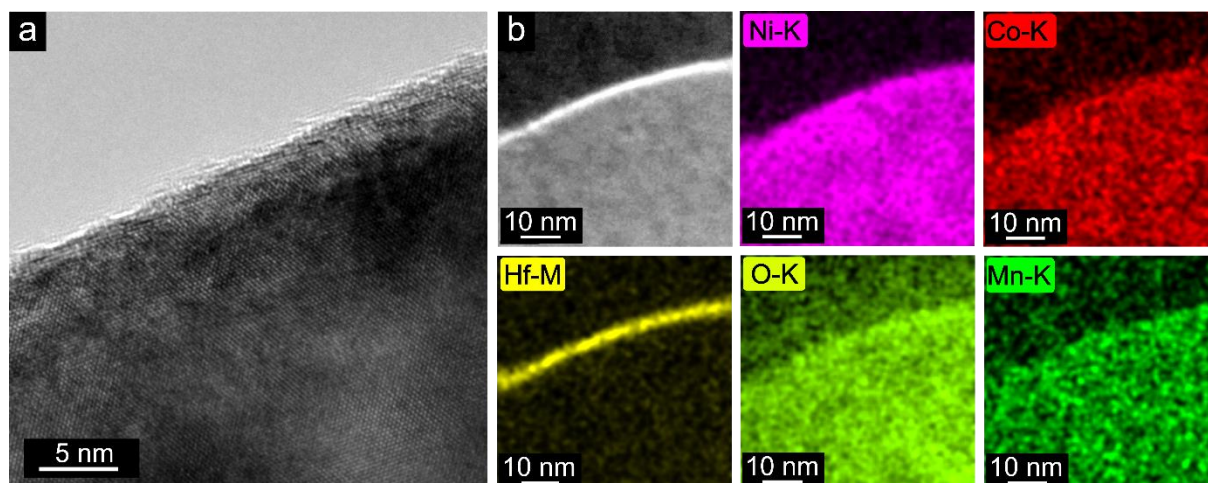


**Figure 2.** Electron microscopy of the annealed  $\text{HfO}_2$ -coated NCM-851005 CAM. (a) HRTEM image showing the particle surface. (b) HAADF STEM image and corresponding elemental maps of a FIB-cut cross section.

### 3.2. Electrochemical Testing and Post-Mortem Analysis

The cycling performance of the uncoated (bare) and  $\text{HfO}_2$ -coated NCM-851005 CAMs was tested in a voltage range of ~2.9-4.3 V versus  $\text{Li}^+/\text{Li}$  at 45 °C in SSB cells with carbon-coated  $\text{Li}_4\text{Ti}_5\text{O}_{12}$  as anode active material and with argyrodite  $\text{Li}_6\text{PS}_5\text{Cl}$  SE, both in the electrode composites and as separator layer (analogous data for the bare NCM-851005 CAM in liquid-electrolyte-based LIB coin cells are presented in **Figure S12**). **Figure 3a** shows the respective first-cycle charge/discharge curves at a rate of 0.1C. The shape of the voltage profiles was virtually identical, differing only slightly at the end of the discharge cycle. As is evident from **Figure 3b**, the larger specific discharge capacity delivered by the  $\text{HfO}_2$ -coated NCM-851005 CAMs is due to the lower irreversibility in the initial cycle and improved kinetics. Comparison of the voltage

profiles further revealed a significantly lower overpotential for the cells using the annealed HfO<sub>2</sub>-coated NCM-851005. As a result, both a slightly larger specific charge capacity (improved delithiation at voltages above 4.0 V vs Li<sup>+</sup>/Li) and a more than 10% increase in specific discharge capacity to over 200 mAh/g<sub>CAM</sub> (~2.1 mAh/cm<sup>2</sup>) were achieved. Note that (uncoated) as-prepared O<sub>3</sub>-treated and annealed O<sub>3</sub>-treated reference samples also delivered larger specific discharge capacities, with increased Coulombic efficiency and rate capability, than the pristine CAM (**Figure S13**). In case of the as-prepared HfO<sub>2</sub>-coated NCM851005, the exposure to ozone during ALD might therefore partly explain the improved cyclability. However, among the annealed CAMs, the HfO<sub>2</sub>-coated NCM851005 clearly outperformed the uncoated counterpart.

An important aspect of the superior electrochemical performance of the annealed HfO<sub>2</sub>-coated NCM-851005 CAM is the considerably increased first-cycle Coulombic efficiency (~88% compared to ~83 and 81% for as-prepared HfO<sub>2</sub>-coated and uncoated NCM-851005, respectively). The differences in Coulombic efficiency point to a different extent of side reactions, especially in the initial cycles. In other words, the higher the reversibility, the lower the level of SE oxidation. **Figure 3c** shows the Coulombic efficiency over the first 20 cycles of identical cells cycled at a rate of 0.5C. The annealed HfO<sub>2</sub>-coated NCM-851005 CAM showed the highest Coulombic efficiencies, also after the first cycle, stabilizing at ~99.5% from the 10<sup>th</sup> cycle onwards, compared to more than 15 cycles for cells using the uncoated or as-prepared HfO<sub>2</sub>-coated NCM-851005. Overall, these findings are characteristic of a more rapid formation of “stable” interfaces when using the annealed HfO<sub>2</sub>-coated NCM-851005 CAM, which also helps explain the reduced overpotential during battery operation.

**Figure 3d** shows the specific discharge capacities for the different NCM-851005 CAMs at rates ranging from 0.1C to 1C (analogous data for the O<sub>3</sub>-treated reference samples are presented in **Figure S14**). As can be seen, the rate performance was clearly improved by the surface coating. At low C-rates, the annealed HfO<sub>2</sub>-coated NCM-851005 delivered significantly larger specific discharge capacities (by 20-30 mAh/g<sub>CAM</sub>) compared to the uncoated and as-prepared HfO<sub>2</sub>-coated NCM-851005 CAMs. Cells using the latter materials delivered similar capacities. However, they diverged with increasing C-rate. At 1C, the improvement in specific discharge capacity achieved by applying a coating amounted to 30% for the as-prepared HfO<sub>2</sub>-coated NCM-851005 and 80% for the annealed HfO<sub>2</sub>-coated NCM-851005. This is probably due, in part, to mitigated effects of interfacial side reactions, which predominantly occur in the initial cycles. Note that interfacial SE degradation has been shown to cause impedance increase.<sup>5,8,9,40–42</sup> Apart from that, the significantly larger cell capacities achieved with the annealed HfO<sub>2</sub>-coated NCM-851005, especially at higher C-rates, indicate improved charge transport across the CAM/SE interface. One possible explanation for this might be the reaction of residual Li species on the surface of the NCM-851005 particles with HfO<sub>2</sub> to form ternary oxides of Li, Hf, and O, which is supported by the XPS results discussed above. Such Li<sub>x</sub>Hf<sub>y</sub>O<sub>z</sub> compounds may contribute to increased ionic conductivity (relative to the binary oxide coating), as has been shown, for example, for Al<sub>2</sub>O<sub>3</sub>.<sup>39</sup> However, the transformation of the crystalline coating into an amorphous surface layer, as evidenced by TEM, might also play a role. For LiNbO<sub>3</sub>, a

well-established CAM coating material, it has been shown that the ionic conductivity is higher, by several orders of magnitude, in the amorphous versus the crystalline state.<sup>43,44</sup>

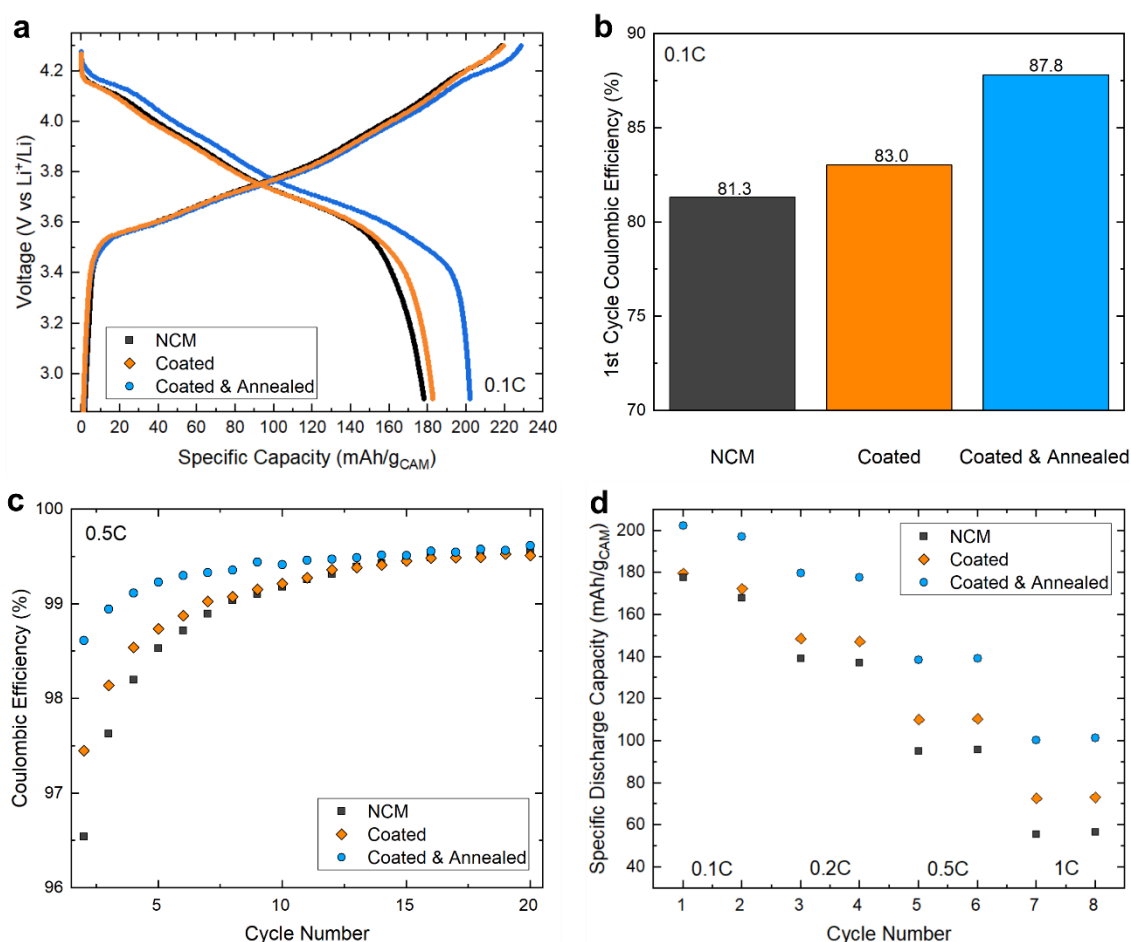


**Figure 3.** Electrochemical performance of the bare and (as-prepared and annealed) HfO<sub>2</sub>-coated NCM-851005 CAMs in SSB cells at 45 °C. (a) First-cycle voltage profiles and (b) initial Coulombic efficiencies at 0.1C. (c) Coulombic efficiencies at 0.5C in the second to 20<sup>th</sup> cycles. (d) Specific discharge capacities at rates ranging from 0.1C to 1C.

Finally, the cycling stability of the uncoated and HfO<sub>2</sub>-coated NCM-851005 CAMs was tested at a rate of 0.5C over 60 cycles (**Figure 4a**). As expected from the data shown in **Figure 3**, the first-cycle specific discharge capacity differed significantly among the different SSB cells ( $q_{dis} \approx 134$  mAh/g<sub>CAM</sub> [uncoated NCM-851005], 155 mAh/g<sub>CAM</sub> [as-prepared HfO<sub>2</sub>-coated NCM-851005], and 170 mAh/g<sub>CAM</sub> [annealed HfO<sub>2</sub>-coated NCM-851005]). While the annealed HfO<sub>2</sub>-coated NCM-851005 showed a rather linear capacity fading behavior (~0.3% per cycle), more rapid decay in the initial 10 cycles, followed by linear capacity degradation, was observed for both the as-prepared HfO<sub>2</sub>-coated NCM-851005 and the uncoated NCM-851005. This confirms the longer time needed to form robust interfaces in the positive electrode when using the latter CAMs. The capacity retention after 60 cycles increased from ~76 to 78% by ALD coating of HfO<sub>2</sub> and further to ~82% (~139 mAh/g<sub>CAM</sub> or ~1.5 mAh/cm<sup>2</sup>) by post annealing at 400

°C, despite the fact that the total cumulative charge passing through the cell was much larger. Overall, stabilization of the CAM/SE interface by applying a coating on the surface of the NCM-851005 secondary particles via ALD is clearly beneficial to the cycling performance and stability of the bulk-type SSB cells.

Cross-sectional SEM imaging and EDS mapping of the cathode of cells using the annealed HfO<sub>2</sub>-coated NCM-851005 before and after cycling revealed that the structure and morphology remain largely unaffected, without apparent loss of contact between the CAM and SE particles (**Figures S15-17**). Furthermore, electrochemical impedance spectroscopy (EIS) measurements were conducted on the SSB cells after 60 cycles. **Figure 4b** shows representative Nyquist plots of the electrochemical impedance, which can be used for semi-quantitative comparisons. As is evident from the depressed semicircle, the difference in cathode interfacial impedance between the uncoated and as-prepared HfO<sub>2</sub>-coated NCM-851005 CAMs was minor. However, a significantly smaller semicircle was found for the annealed HfO<sub>2</sub>-coated NCM-851005, corroborating the results from the above cycling experiments.

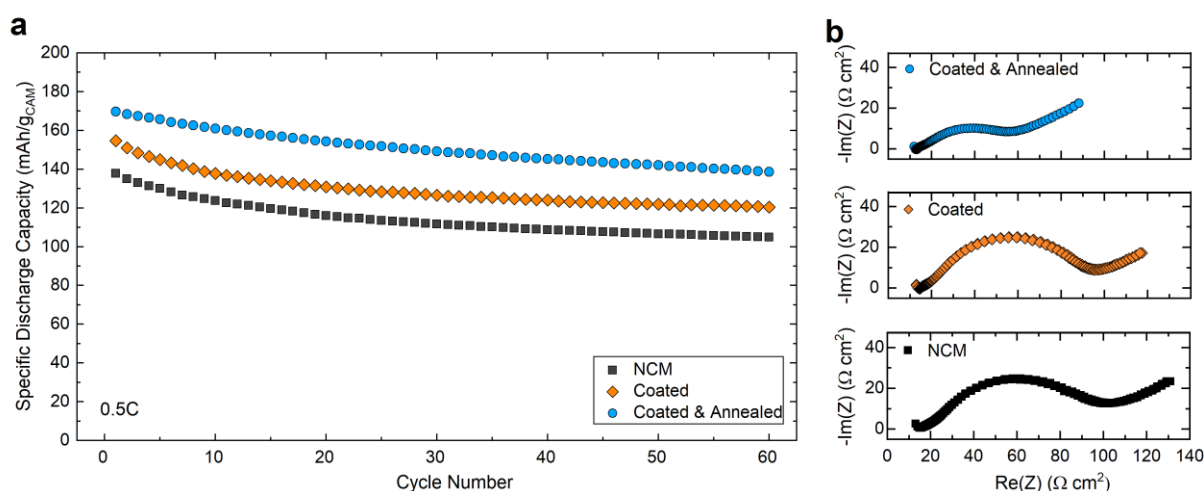


**Figure 4.** Long-term cycling performance of the bare and (as-prepared and annealed) HfO<sub>2</sub>-coated NCM-851005 CAMs in SSB cells at 45 °C. (a) Specific discharge capacities at 0.5C over the first 60 cycles. (b) Nyquist plots of the electrochemical impedance at 45 °C for the different cells after cycling.

## 4. Conclusions

High-quality, ALD-derived HfO<sub>2</sub> coatings onto NCM-851005 CAM, achieved by sequential surface reactions of H<sub>2</sub>O, or preferably O<sub>3</sub>, and TEMAH at 250 °C, have been presented. TEM measurements indicated that the as-deposited HfO<sub>2</sub> is nanocrystalline, but can be modified by a facile post treatment in O<sub>2</sub> atmosphere at 400 °C, resulting in a smooth (amorphous) Hf-containing surface layer of thickness 2-3 nm. Electrochemical testing demonstrated the positive effect that HfO<sub>2</sub> ALD coating has on the cycling performance and stability of the NCM-851005 CAM in SSB cells. The cyclability was considerably improved by annealing of the coated material. We suggest the reaction of lithium residues on the NCM surface with HfO<sub>2</sub> to form Li-based

ternary oxides as the most likely cause for such improvement, but this needs further study. The present work is one of the first demonstrations of the unique capabilities of ALD to produce ultrathin, conformal CAM coatings for bulk-type SSB applications. The results are encouraging and call for future investigations into other (Li-containing) materials to improve on the understanding of the functioning of protective coatings in solid-state and other batteries.

## **Associated Content**

### **Supporting Information**

Cycling performance of the NCM-851005 coated by ALD of TEMAH/H<sub>2</sub>O or TEMAH/O<sub>3</sub> (for 0, 10, 20, and 100 ALD cycles); HfO<sub>2</sub> content from ICP-OES versus ALD cycles; XRD patterns collected from the NCM-851005 before and after coating and Rietveld refinement profile for the bare NCM-851005; refined structural parameters; O 1s and Ni 2p core-level spectra for the bare and HfO<sub>2</sub>-coated NCM-851005 before/after heating; high- and low-magnification SEM images of the bare and HfO<sub>2</sub>-coated NCM-851005 before/after heating; XP spectra of the Hf 4d and 4f core-level regions for the HfO<sub>2</sub>-coated NCM-851005 before/after heating; calculation of lattice spacings from HRTEM images; determination of the coating thickness, EDS data, and mapping results for the annealed HfO<sub>2</sub>-coated NCM-851005; cycling performance of the bare NCM-851005 in liquid-electrolyte-based LIB coin cells; cycling performance of the O<sub>3</sub>-treated (uncoated) NCM-851005 before/after heating; cross-sectional SEM imaging and EDS mapping of the cathode and cathode/separator interface of SSB cells using the annealed HfO<sub>2</sub>-coated NCM-851005 before/after cycling.

## **Author Information**

### **Corresponding Authors**

\*Phone: +49 721 60828827; Email: [juergen.janek@kit.edu](mailto:juergen.janek@kit.edu)

\*Phone: +49 721 60828827; Email: [torsten.brezesinski@kit.edu](mailto:torsten.brezesinski@kit.edu)

## **Notes**

The authors declare no competing financial interest.

## **Acknowledgements**

This study was supported by BASF SE. The work was partly performed with the support of the Karlsruhe Nano Micro Facility (KNMF), a Helmholtz Research Infrastructure at Karlsruhe Institute of Technology (KIT). D. K. acknowledges financial support from Fonds der Chemischen Industrie (FCI) through a Kekulé scholarship. We thank Dr. Thomas Bergfeldt (Institute for Applied Materials, KIT) for ICP-OES measurements, Dr. Andrey Mazilkin (Institute of Nanotechnology, KIT) for TEM

support, Thomas Diemant (Ulm University) for XPS support, as well as Prof. Christian Kübel (Institute of Nanotechnology, KIT) and Dr. Xiaohan Wu (BASF SE) for fruitful discussions.

## References

- (1) Janek, J.; Zeier, W. G. A Solid Future for Battery Development. *Nat. Energy* **2016**, *1*, 16141.
- (2) Andre, D.; Kim, S.-J.; Lamp, P.; Lux, S. F.; Maglia, F.; Paschos, O.; Stiaszny, B. Future Generations of Cathode Materials: An Automotive Industry Perspective. *J. Mater. Chem. A* **2015**, *3*, 6709–6732.
- (3) Randau, S.; Weber, D. A.; Kötz, O.; Koerver, R.; Braun, P.; Weber, A.; Ivers-Tiffée, E.; Adermann, T.; Kulisch, J.; Zeier, W. G.; Richter, F. H.; Janek, J. Benchmarking the Performance of All-Solid-State Lithium Batteries. *Nat. Energy* **2020**, *5*, 259–270.
- (4) Wang, Y.; Richards, W. D.; Ong, S. P.; Miara, L. J.; Kim, J. C.; Mo, Y.; Ceder, G. Design Principles for Solid-State Lithium Superionic Conductors. *Nat. Mater.* **2015**, *14*, 1026–1031.
- (5) Banerjee, A.; Wang, X.; Fang, C.; Wu, E. A.; Meng, Y. S. Interfaces and Interphases in All-Solid-State Batteries with Inorganic Solid Electrolytes. *Chem. Rev.* **2020**, *120*, 6878–6933.
- (6) Sun, Y.-K. Promising All-Solid-State Batteries for Future Electric Vehicles. *ACS Energy Lett.* **2020**, *5*, 3221–3223.
- (7) Lim, H.-D.; Park, J.-H.; Shin, H.-J.; Jeong, J.; Kim, J. T.; Nam, K.-W.; Jung, H.-G.; Chung, K. Y. A Review of Challenges and Issues Concerning Interfaces for All-Solid-State Batteries. *Energy Storage Mater.* **2020**, *25*, 224–250.
- (8) Culver, S. P.; Koerver, R.; Zeier, W. G.; Janek, J. On the Functionality of Coatings for Cathode Active Materials in Thiophosphate-Based All-Solid-State Batteries. *Adv. Energy Mater.* **2019**, *9*, 1900626.
- (9) Strauss, F.; Stepien, D.; Maibach, J.; Pfaffmann, L.; Indris, S.; Hartmann, P.; Brezesinski, T. Influence of Electronically Conductive Additives on the Cycling Performance of Argyrodite-Based All-Solid-State Batteries. *RSC Adv.* **2020**, *10*, 1114–1119.
- (10) Kim, A.-Y.; Strauss, F.; Bartsch, T.; Teo, J. H.; Hatsukade, T.; Mazilkin, A.; Janek, J.; Hartmann, P.; Brezesinski, T. Stabilizing Effect of a Hybrid Surface Coating on a Ni-Rich NCM Cathode Material in All-Solid-State Batteries. *Chem. Mater.* **2019**, *31*, 9664–9672.
- (11) Takada, K.; Ohta, N.; Zhang, L.; Fukuda, K.; Sakaguchi, I.; Ma, R.; Osada, M.; Sasaki, T. Interfacial Modification for High-Power Solid-State Lithium Batteries. *Solid State Ionics* **2008**, *179*, 1333–1337.
- (12) Oh, G.; Hirayama, M.; Kwon, O.; Suzuki, K.; Kanno, R. Bulk-Type All Solid-State Batteries with 5 V Class  $\text{LiNi}_{0.5}\text{Mn}_{1.5}\text{O}_4$  Cathode and  $\text{Li}_{10}\text{GeP}_2\text{S}_{12}$  Solid Electrolyte. *Chem. Mater.* **2016**, *28*, 2634–2640.
- (13) Weber, D.; Tripković, Đ.; Kretschmer, K.; Bianchini, M.; Brezesinski, T. Surface Modification Strategies for Improving the Cycling Performance of Ni-Rich

- Cathode Materials. *Eur. J. Inorg. Chem.* **2020**, 2020, 3117–3130.
- (14) Park, J. S.; Mane, A. U.; Elam, J. W.; Croy, J. R. Amorphous Metal Fluoride Passivation Coatings Prepared by Atomic Layer Deposition on LiCoO<sub>2</sub> for Li-Ion Batteries. *Chem. Mater.* **2015**, 27, 1917–1920.
  - (15) Xie, J.; Sendek, A. D.; Cubuk, E. D.; Zhang, X.; Lu, Z.; Gong, Y.; Wu, T.; Shi, F.; Liu, W.; Reed, E. J.; Cui, Y. Atomic Layer Deposition of Stable LiAlF<sub>4</sub> Lithium Ion Conductive Interfacial Layer for Stable Cathode Cycling. *ACS Nano* **2017**, 11, 7019–7027.
  - (16) Neudeck, S.; Mazilkin, A.; Reitz, C.; Hartmann, P.; Janek, J.; Brezesinski, T. Effect of Low-Temperature Al<sub>2</sub>O<sub>3</sub> ALD Coating on Ni-Rich Layered Oxide Composite Cathode on the Long-Term Cycling Performance of Lithium-Ion Batteries. *Sci. Rep.* **2019**, 9, 5328.
  - (17) Mohanty, D.; Dahlberg, K.; King, D. M.; David, L. A.; Sefat, A. S.; Wood, D. L.; Daniel, C.; Dhar, S.; Mahajan, V.; Lee, M.; Albano, F. Modification of Ni-Rich FCG NMC and NCA Cathodes by Atomic Layer Deposition: Preventing Surface Phase Transitions for High-Voltage Lithium-Ion Batteries. *Sci. Rep.* **2016**, 6, 26532.
  - (18) Zhao, Y.; Zheng, K.; Sun, X. Addressing Interfacial Issues in Liquid-Based and Solid-State Batteries by Atomic and Molecular Layer Deposition. *Joule* **2018**, 2, 2583-2604.
  - (19) Wang, B.; Zhao, Y.; Banis, M. N.; Sun, Q.; Adair, K. R.; Li, R.; Sham, T.-K.; Sun, X. Atomic Layer Deposition of Lithium Niobium Oxides as Potential Solid-State Electrolytes for Lithium-Ion Batteries. *ACS Appl. Mater. Interfaces* **2018**, 10, 1654–1661.
  - (20) Liu, J.; Banis, M. N.; Li, X.; Lushington, A.; Cai, M.; Li, R.; Sham, T.-K.; Sun, X. Atomic Layer Deposition of Lithium Tantalate Solid-State Electrolytes. *J. Phys. Chem. C* **2013**, 117, 20260–20267.
  - (21) Kozen, A. C.; Pearse, A. J.; Lin, C.-F.; Noked, M.; Rubloff, G. W. Atomic Layer Deposition of the Solid Electrolyte LiPON. *Chem. Mater.* **2015**, 27, 5324–5331.
  - (22) Woo, J. H.; Trevey, J. E.; Cavanagh, A. S.; Choi, Y. S.; Kim, S. C.; George, S. M.; Oh, K. H.; Lee, S.-H. Nanoscale Interface Modification of LiCoO<sub>2</sub> by Al<sub>2</sub>O<sub>3</sub> Atomic Layer Deposition for Solid-State Li Batteries. *J. Electrochem. Soc.* **2012**, 159, A1120–A1124.
  - (23) Ito, S.; Fujiki, S.; Yamada, T.; Aihara, Y.; Park, Y.; Kim, T. Y.; Baek, S.-W.; Lee, J. M.; Doo, S.; Machida, N. A Rocking Chair Type All-Solid-State Lithium Ion Battery Adopting Li<sub>2</sub>O-ZrO<sub>2</sub> Coated LiNi<sub>0.8</sub>Co<sub>0.15</sub>Al<sub>0.05</sub>O<sub>2</sub> and a Sulfide Based Electrolyte. *J. Power Sources* **2014**, 248, 943–950.
  - (24) Lee, Y.-G.; Fujiki, S.; Jung, C.; Suzuki, N.; Yashiro, N.; Omoda, R.; Ko, D.-S.; Shiratsuchi, T.; Sugimoto, T.; Ryu, S.; Ku, J. H.; Watanabe, T.; Park, Y.; Aihara, Y.; Im, D.; Han, I. T. High-Energy Long-Cycling All-Solid-State Lithium Metal Batteries Enabled by Silver-Carbon Composite Anodes. *Nat. Energy* **2020**, 5, 299–308.
  - (25) Wang, C.; Chen, L.; Zhang, H.; Yang, Y.; Wang, F.; Yin, F.; Yang, G. Li<sub>2</sub>ZrO<sub>3</sub> Coated LiNi<sub>1/3</sub>Co<sub>1/3</sub>Mn<sub>1/3</sub>O<sub>2</sub> for High Performance Cathode Material in Lithium Batteries. *Electrochim. Acta* **2014**, 119, 236–242.
  - (26) Strauss, F.; Teo, J. H.; Maibach, J.; Kim, A.-Y.; Mazilkin, A.; Janek, J.;

- Brezesinski, T. Li<sub>2</sub>ZrO<sub>3</sub>-Coated NCM622 for Application in Inorganic Solid-State Batteries: Role of Surface Carbonates in the Cycling Performance. *ACS Appl. Mater. Interfaces* **2020**, *12*, 57146–57154.
- (27) Kukli, K.; Ritala, M.; Sajavaara, T.; Keinonen, J.; Leskelä, M. Atomic Layer Deposition of Hafnium Dioxide Films from Hafnium Tetrakis(Ethylmethanamide) and Water. *Chem. Vap. Deposition* **2002**, *8*, 199–205.
- (28) Senzaki, Y.; Park, S.; Chatham, H.; Bartholomew, L.; Nieveen, W. Atomic Layer Deposition of Hafnium Oxide and Hafnium Silicate Thin Films Using Liquid Precursors and Ozone. *J. Vac. Sci. Technol., A* **2004**, *22*, 1175–1181.
- (29) Kirsch, P. D.; Quevedo-Lopez, M. A.; Li, H.-J.; Senzaki, Y.; Peterson, J. J.; Song, S. C.; Krishnan, S. A.; Moumen, N.; Barnett, J.; Bersuker, G.; Hung, P. Y.; Lee, B. H.; Lafford, T.; Wang, Q.; Gay, D.; Ekerdt, J. G. Nucleation and Growth Study of Atomic Layer Deposited HfO<sub>2</sub> Gate Dielectrics Resulting in Improved Scaling and Electron Mobility. *J. Appl. Phys.* **2006**, *99*, 023508.
- (30) Liu, X.; Ramanathan, S.; Longdergan, A.; Srivastava, A.; Lee, E.; Seidel, T. E.; Barton, J. T.; Pang, D.; Gordon, R. ALD of Hafnium Oxide Thin Films from Tetrakis(Ethylmethanamino)Hafnium and Ozone. *J. Electrochem. Soc.* **2005**, *152*, G213–G219.
- (31) Rose, M.; Niinistö, J.; Endler, I.; Bartha, J. W.; Kücher, P.; Ritala, M. In Situ Reaction Mechanism Studies on Ozone-Based Atomic Layer Deposition of Al<sub>2</sub>O<sub>3</sub> and HfO<sub>2</sub>. *ACS Appl. Mater. Interfaces* **2010**, *2*, 347–350.
- (32) Toby, B. H.; Von Dreele, R. B. GSAS-II: The Genesis of a Modern Open-Source All Purpose Crystallography Software Package. *J. Appl. Crystallogr.* **2013**, *46*, 544–549.
- (33) Kim, A.-Y.; Strauss, F.; Bartsch, T.; Teo, J. H.; Janek, J.; Brezesinski, T. Effect of Surface Carbonates on the Cyclability of LiNbO<sub>3</sub>-Coated NCM622 in All-Solid-State Batteries with Lithium Thiophosphate Electrolytes. *Sci. Rep.* **2021**, *11*, 5367.
- (34) Jung, R.; Morasch, R.; Karayaylali, P.; Phillips, K.; Maglia, F.; Stinner, C.; Shao-Horn, Y.; Gasteiger, H. A. Effect of Ambient Storage on the Degradation of Ni-Rich Positive Electrode Materials (NMC811) for Li-Ion Batteries. *J. Electrochem. Soc.* **2018**, *165*, A132–A141.
- (35) Sønsteby, H. H.; Yanguas-Gil, A.; Elam, J. W. Consistency and Reproducibility in Atomic Layer Deposition. *J. Vac. Sci. Technol., A* **2020**, *38*, 020804.
- (36) Geller, S.; Corenzwit, E. Hafnium Oxide, HfO<sub>2</sub> (Monoclinic). *Anal. Chem.* **1953**, *25*, 1774.
- (37) Richey, N. E.; De Paula, C.; Bent, S. F. Understanding Chemical and Physical Mechanisms in Atomic Layer Deposition. *J. Chem. Phys.* **2020**, *152*, 040902.
- (38) Hoskins, A. L.; McNeary, W. W.; Millican, S. L.; Gossett, T. A.; Lai, A.; Gao, Y.; Liang, X.; Musgrave, C. B.; Weimer, A. W. Nonuniform Growth of Sub-2 Nanometer Atomic Layer Deposited Alumina Films on Lithium Nickel Manganese Cobalt Oxide Cathode Battery Materials. *ACS Appl. Nano Mater.* **2019**, *2*, 6989–6997.
- (39) Negi, R. S.; Celik, E.; Pan, R.; Stäglich, R.; Senker, J.; Elm, M. T. Insights into the Positive Effect of Post-Annealing on the Electrochemical Performance of Al<sub>2</sub>O<sub>3</sub>-Coated Ni-Rich NCM Cathodes for Lithium-Ion Batteries. *ACS Appl.*

*Energy Mater.* **2021**, *4*, 3369–3380.

- (40) Auvergniot, J.; Cassel, A.; Ledeuil, J.-B.; Viallet, V.; Seznec, V.; Dedryvère, R. Interface Stability of Argyrodite  $\text{Li}_6\text{PS}_5\text{Cl}$  toward  $\text{LiCoO}_2$ ,  $\text{LiNi}_{1/3}\text{Co}_{1/3}\text{Mn}_{1/3}\text{O}_2$ , and  $\text{LiMn}_2\text{O}_4$  in Bulk All-Solid-State Batteries. *Chem. Mater.* **2017**, *29*, 3883–3890.
- (41) Walther, F.; Koerver, R.; Fuchs, T.; Ohno, S.; Sann, J.; Rohnke, M.; Zeier, W. G.; Janek, J. Visualization of the Interfacial Decomposition of Composite Cathodes in Argyrodite-Based All-Solid-State Batteries Using Time-of-Flight Secondary-Ion Mass Spectrometry. *Chem. Mater.* **2019**, *31*, 3745–3755.
- (42) Walther, F.; Strauss, F.; Wu, X.; Mogwitz, B.; Hertle, J.; Sann, J.; Rohnke, M.; Brezesinski, T.; Janek, J. The Working Principle of a  $\text{Li}_2\text{CO}_3/\text{LiNbO}_3$  Coating on NCM for Thiophosphate-Based All-Solid-State Batteries. *Chem. Mater.* **2021**, *33*, 2110–2125.
- (43) Glass, A. M.; Nassau, K.; Negran, T. J. Ionic Conductivity of Quenched Alkali Niobate and Tantalate Glasses. *J. Appl. Phys.* **1978**, *49*, 4808–4811.
- (44) Ohta, N.; Takada, K.; Sakaguchi, I.; Zhang, L.; Ma, R.; Fukuda, K.; Osada, M.; Sasaki, T.  $\text{LiNbO}_3$ -Coated  $\text{LiCoO}_2$  as Cathode Material for All Solid-State Lithium Secondary Batteries. *Electrochem. Commun.* **2007**, *9*, 1486–1490.

### TOC Graphic

